


Influences and Effects on Scaling the Pressure Stiffness of Additively Manufactured Meso Structures

F. Schulte , L. Sauerzapf and E. Kirchner

Technical University of Darmstadt, Germany

 schulte@pmd.tu-darmstadt.de

Abstract

AM-meso structures offer a high potential for adapted properties combined with lightweight design. To utilize the potential a purposeful design of the meso structures is required. Therefore, this contribution presents an approach for modelling their properties depending on design parameters by scaling relationships. The relationships are investigated based on grey box and axiomatic models of elementary cells. Exemplary the pressure stiffness is determined using FEM in comparison to an analytical approximation. The comparison reveals effects and influences occurring within the elementary cell.

Keywords: additive manufacturing, characteristics and properties, meso structures, scaling, modelling

1. Introduction

Products satisfy manifold requirements cross-application. One possibility for realising required functions is the use of inner structures within volumetric components like in the crash helmet or foot prosthesis shown in Figure 1, while the outer cover is customised for the user and the outer conditions. The design of the inner structure enables the realisation of required properties like a defined stiffness and damping with low weight and material expenses at the same time. The inner structure is characterised by the periodicity of elementary structures, which are locally adapted to the particular requirements. The structural size is on the meso scale between 0.1 and 10 mm (Nguyen et al., 2013), which gives them the name meso structure. The design freedom of additive manufacturing enables to realise determinate, regular structures with a defined topology, elementary structure size, thickness and orientation. Purposefully grading the structures creates local properties (Steffan et al., 2021; Steffan et al., 2020). The potentials of meso structures used for the examples are the separation of the outer shape and the inner properties combined with the full surface support of the outer shell.

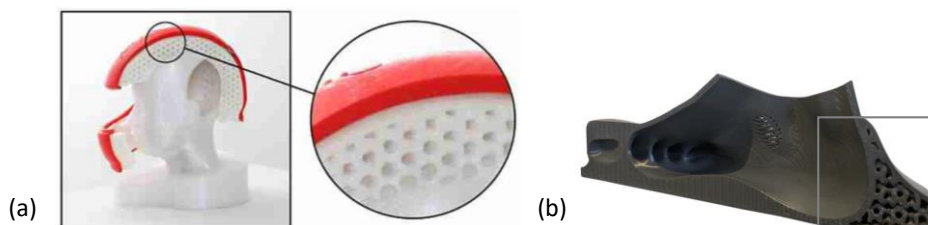


Figure 1. Exemplary applications of additively manufactured meso structures: inner shell of a crash helmet (a) (Steffan et al., 2020) part of a foot-prosthesis (b) (Steffan et al., 2021)

To purposefully design the meso structures, in this contribution the identification of design parameters, effects influencing their properties and a mathematical model for scaling the properties depending on the

design parameters are aspired. To achieve the mathematical model, simulation results of the pressure stiffness of meso structures are fitted using different mathematical functions. Furthermore, an analytical model of two common elementary cells is derived to identify underlying effects of the elementary cell's geometry on the stiffness, to improve the mathematical model by considering the effects.

2. Fundamentals

Additively manufactured meso structures are examined in different applications to achieve lightweight design in combination with properties like vibration damping or thermal conductivity in literature (Maconachie et al., 2019; Hao et al., 2011). In Finite Element simulations or experiments the properties of selected meso structures are investigated in comparison rather than an overview over different meso structures and their properties is given. (Ge et al., 2018; Vega-Moreno et al., 2020).

2.1. Additively manufactured meso structures

Meso structures are defined by the size of the elementary structure in the meso scale (Nguyen et al., 2013). The additively manufactured meso structures are furthermore characterised by the repeated arrangement of identical elementary cells, which are the smallest repeated indivisible structure unit. The meso structures comprise strut, plate and shell lattice structures differentiated by their basic geometric elements. The elementary cell types can be arranged in e.g. face or body centred cubic structures as shown for strut lattices in Figure 2 (Maconachie et al., 2019). The variety of elementary cells allows to choose and adapt the cells for a broad range of properties and therefore possibilities of application.

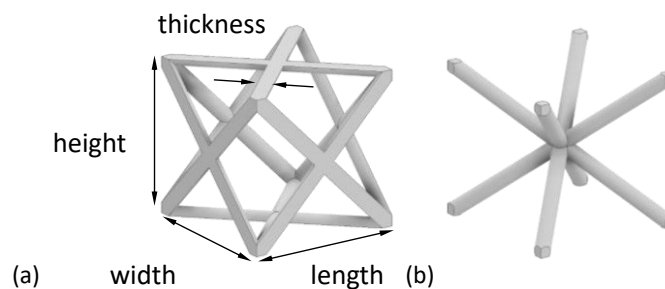


Figure 2. Face centred cubic (FCC) strut lattice cell with geometrical design parameters of a meso structure elementary cell (a) and body centred cubic (BCC) strut lattice cell (b)

2.2. Influencing parameters on additively manufactured meso structures

Schulte et al. (2021) identified influencing parameters based on the consideration of two dimensional frameworks and strut cells they consist of. The influencing parameters are classified into material, geometry and topology. The meso structure's material influences its properties with the Young's modulus and Poisson's ratio. The geometrical influences are length, width and height of the enveloping cuboid of the elementary cell and the structural thickness, which e.g. is the strut diameter for strut lattices. The design parameters are exemplary depicted for a face centred cubic (FCC) strut lattice in Figure 2. The relations of the design parameters influence the properties through asymmetry effects of length to width, width to height and height to length ratio and the structural thickness to the characteristic length of the envelope. The topology describes the distribution of the material in the elementary cell volume, i.e. shape and placement of e.g. the struts (Schulte et al., 2021; Lachmayer and Lippert, 2020).

The mechanical properties of meso structured components are frequently designated as equivalent continuum properties, mainly the equivalent Young's modulus E^* and relative density ρ^* . The impact of the influencing parameters on the equivalent properties depends on the load case, which means they have to be defined load-case-specific. The properties of asymmetric elementary cells are anisotropic and need to be described by a tensor (Schulte et al., 2021; Becker and Gross, 2002; Gibson and Ashby, 2010).

Within the compound of cells, additionally the cell's orientation in relation to the component and the segmentation have an impact. The segmentation describes the subdivision of a component into areas filled with different types or dimensions of elementary cells. The division into areas of different meso cells moreover necessitates transitions between the areas, where either the variation of cells has to adhere to

transition conditions or a transition structure has to be developed connecting the areas to ensure maintaining the compound. In case of the similar elementary cell topologies, transition conditions can e.g. be taken from analytical beam theory like the condition of even cross section that is prerequisite for the Bernoulli beam theory. Under these transition conditions, necessary relations of the dimensions for maintaining the cell bond can be deduced for neighbouring elementary cells (Schulte et al., 2021).

2.3. Equivalent continuum properties for the Finite Element Method calculation

For the calculation of meso structure properties and the properties of meso-structured components, currently the Finite Element Method (FEM) is usually used. To streamline the FE-calculation single elementary meso cells are simulated and equivalent continuum properties are determined. The equivalent properties are assigned to the meso-structured volume of a component that is afterwards calculated as a continuum. The calculated properties of the equivalent continuum component allow drawing conclusions to the behaviour of the meso structure (Cheng et al., 2018; Wang et al., 2020).

The comparison of different elementary cells or cell dimensions necessitates the repeated determination of the equivalent continuum properties and conduction of the FE-calculation of the meso structure using the equivalent properties. Purposeful dimensioning requires iteration, consequently.

Within literature different approaches of Finite Element modelling the elementary cells for regular meso structures exist. The investigations in this paper focus on strut lattices which can be modelled as beam or 3D-volume elements. The beam elements solve the load-deformation relationship for the representative volume element (RVE) as the solution of a bending beam and are advantageous in terms of the calculation time. However, their application is restricted to strut lattices and the exact modelling of the strut conjunction is not possible, as the overlapping volume is not considered. Therefore, 3D-volume elements provide higher accuracy of the calculation, in which the load-deformation relationship is solved for simple RVE, like tetrahedral, with known initial functions, accepting a significantly higher calculation time (Dong et al., 2017).

3. Research question

Additively manufactured meso structures offer potentials like locally adapted, defined and combinable properties, e.g. stiffness, damping and low weight, used for the crash helmet and foot prosthesis. To utilise these potentials and make them available for different applications purposeful design of the meso structures is required. Currently the meso structures are modelled in CAD by duplicating similar elementary cells and examined using the homogenisation method for FEM. Using this FEM approach requires orthogonal cell properties and is limited to a (at least zonally) homogeneous meso structure. Furthermore, the usage of FEM requires iterations for the choice of elementary cell type and dimensions, because the FEM does not enable direct access to the underlying influencing design parameters. Hence, dimensioning the parameters for the aspired properties partly bases on trial and error. Thus, a model for dimensioning meso structures omitting iterations is aspired.

Utilising cells with anisotropic properties and an inhomogeneous distribution within the volumetric component enables a further improvement of meso-structured components. The grading of component properties allows adapting to inhomogeneous load distributions and smoothening leaps in stiffness between the meso structure and e.g. solid body parts of a component like an outer shell. The additional modelling expenses are considered as acceptable if the cells can be scaled. However, scaling models for different elementary cells with anisotropic properties are not available, yet. Scaling of anisotropic cells can be investigated based on grey box and axiomatic models of elementary cells. Thereby scaling models understandable and easily applicable for the developer are favourable.

A mathematical description based on physical relations of the relationships between meso structure properties and the influencing design parameters would allow an easier and meaningful calculation of the properties and a direct conclusion from the aspired property value to the necessary design parameter values. This enables a purposeful selection of the elementary cell type, dimensions or structural thickness. To achieve the aspired model this contribution investigates the following research questions:

Which influences and effects determine the properties of meso structure elementary cells?

How do the influences and effects enable scaling of (stiffness) properties originating from a physically motivated analytical model of the relation between design parameters and cell properties?

4. Model for scaling of meso structures properties

The mathematical description for scaling the meso structure properties is determined by fitting the results of a FE-simulation depending on the influencing parameters. To identify underlying effects the FCC and BCC strut lattice cell are approximated by an analytical calculation, whereby the impact of the influencing parameters and further underlying effects are identified.

4.1. Determination of meso structure properties using FEM

The FEM analysis is applicable as a form of grey box model for examining the meso structure properties. Therefore, the theoretical properties of the meso structure elementary cells are simulated using a FE-Model as a data basis for the development of the mathematical scaling model. To approach the desired mathematical description the investigations initially focus on symmetric cubic strut lattice cells inside uniform compounds of equal elementary cells. As the properties are load dependent, the load case of pressure and the property stiffness are chosen. The FE-Model representing a compression test is build with one elementary cell of 10 mm edge length between two rigid plates, as illustrated in Figure 3 (a). The FEM simulations are performed using the Abaqus/Standard software package (Dessault Systèmes, 2020) and the elementary cell is meshed with 10-node quadratic tetrahedron elements with a mesh size of 0.2 mm after a mesh-sensitivity study that ensures convergence of the results. The contact properties between the plates and the elementary cell are set to frictionless in tangential and hard in normal direction. To determine the pressure stiffness, a reference point at the centre of the upper plate is impinged with a displacement, while the lower plate is fixed. Meanwhile the reaction force and the displacement are tracked at the upper reference point and the stiffness of the cell is calculated from the force-displacement diagram using the cell's dimensions. The influence of the neighbouring cells on the considered single cell is regarded by periodic boundary conditions (PBC) that assign opposite nodes to one another and impinge the same node displacement for both sides. The underlying material properties are $E = 71\,000$ MPa and $\nu = 0.3$ based on AlSi10Mg. Smith et al. (2013) have already created a similar model. To evaluate the periodic boundary conditions the tension curve of the single cell and a centred cell in a cell compound as shown in Figure 3 (b), are squared and show close agreement.

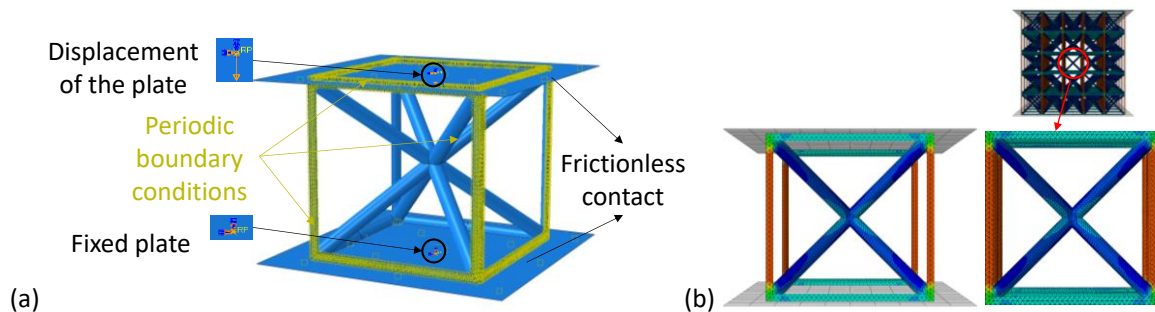


Figure 3. Depiction of the FE-Model (a) comparison of PBCs and a cell compound (b)

4.2. Fitting the results of the FEM

The results of the pressure stiffness are determined depending on the influencing parameters structural thickness d and cell size. Due to the chosen cubic cells the cell size parameters are reduced to the edge length l . The simulation and analytical results are calculated with an edge length of $l = 10$ mm and thickness varied within $0.9 \text{ mm} \leq d \leq 3.5 \text{ mm}$. For the mathematical description, different types of mathematical fits are compared considering their suitability for the simulated curves as well as for the physical interrelations of comparable solid materials. The following types, which have already been considered in literature, are looked at and exemplary shown for the FCC strut lattice in comparison in Figure 4 (Cheng et al., 2018; Cheng et al., 2017; Vega-Moreno et al., 2020; Xu et al., 2016; Nguyen et al., 2021; Crupi et al., 2017; Ruiz de Galarreta et al., 2020):

- Polynomial fit: $y(x) = a_0 + a_1x + a_2x^2 + \dots + a_nx^n$ of first to fourth order
- Power fit: $y(x) = ax^b$

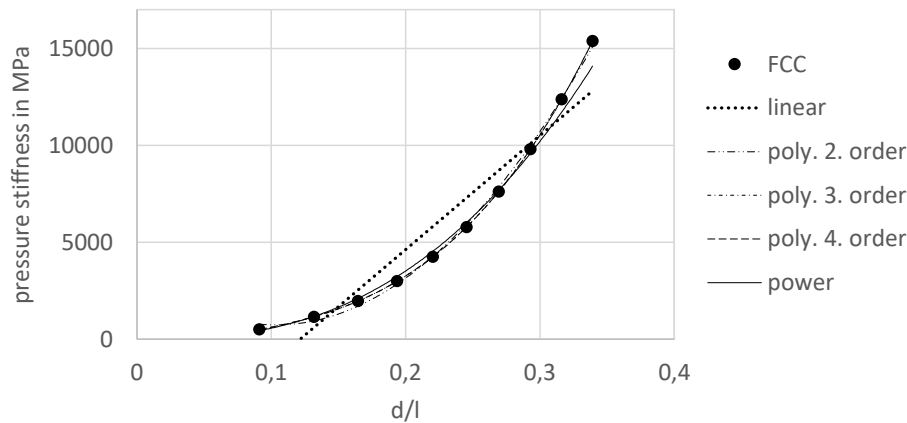


Figure 4. Exemplary comparison of different mathematical fits for FCC strut lattice cell

Further types like exponential fits are omitted in Figure 4 because they are far from suitable for approximating the interrelation of the pressure stiffness (Shi et al., 2021). Out of the polynomial fits the fourth degree shows the best agreement with simulated results for the pressure stiffness judged by the coefficient of determination R^2 , which is calculated using equation (1) (Hradetzky, 1978)

$$R^2 = 1 - \frac{\sum(y_i - \hat{y}_i)^2}{\sum(y_i - \bar{y})^2} \quad (1)$$

y_i : simulated value
 \hat{y}_i : predicted value of the fit function
 \bar{y} : average value

The coefficient of determination is $R^2 = 1$ for polynomial of fourth order, while the power fit has a slightly lower coefficient of $R^2 = 0.99$. The power fit though offers an advantage regarding the physical backgrounds because different from the polynomial fit the power function is invertible like stiffness and yieldingness or if d/l is reversed to l/d . Another advantage is the possibility to utilise the power fit for scaling applying similarity relations. Therefore, the power fit is looked at in the following.

Figure 5 shows the simulation results and power fits for variations of BCC and FCC strut lattice cells and their combination the FBCC strut lattice depending on d/l . The graphs show that the power fit is applicable for different strut lattices but depending on the elementary cell topology, the accuracy of the approximation varies. Furthermore, the pressure stiffness of each cell type follows an individual function.

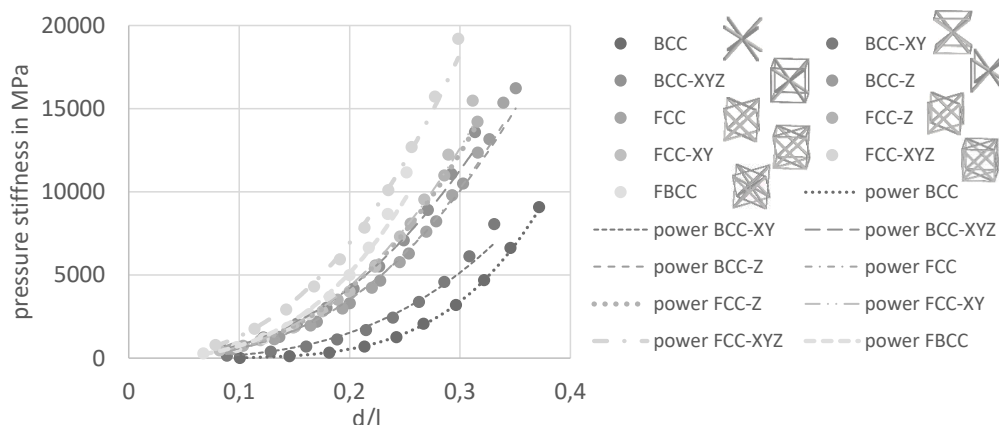


Figure 5. Power fit of pressure stiffness of different strut lattice cells as a function of d/l ratio

4.3. Analytical calculation of FCC and BCC elementary strut lattice cell

The relationships and growth exponents derived from the FEM analysis do not provide physically comprehensible and valid scaling laws even for orthotropic elementary cells. Hence, solely considering the FEM analysis' results provides no clear scaling relations. The zonally differing behaviour though indicates the superposition of several effects within the elementary cell. Aim of the

analytical analysis of the BCC and FCC strut lattice cells is to identify relevant influences and effects and to quantify them for the aspired scaling model. In comparison to the simulated compressive stiffness results, the FCC and the BCC strut lattice elementary cell are therefore approximated using analytical calculation approaches. The FCC and BCC cell are initially chosen because of their manageable topology. For the analytical calculation of the FCC and BCC cells, several assumption are made, which are transferred from known similar structures and load and boundary conditions where the assumptions have proven to be valid:

- Originating from the symmetry of the cell one eighth of the cell composed of two spatially orthogonal, symmetrically loaded frameworks is analysed regarding appropriate boundary conditions and half the force on each of the frameworks (Figure 6 (a))
- Full cross sections are used to calculate inner struts, half the cross sections for side struts
- The flow of force is separated into two independent parallel paths for the FCC cell like shown in Figure 6 (b) and (c) (equation (2), (7)), which comprise the assumptions of bending and additional significant deformation due to shear of a Timoshenko beam and are applicable for different length to diameter ratios:
 - a framework, which transfers the part of the force via tension and pressure (equation (3), (5))
 - a statically overdetermined bending beam, which transfers part of the force via bending, shear and a normal compression (equation (4), (6))
- The horizontal displacement of both force paths is identical to ensure cohesion of the struts
- The BCC cell is calculated as only the statically overdetermined bending beam clamped on both sides additionally considering shear and pressure by a normal force like in Figure 6 (c)

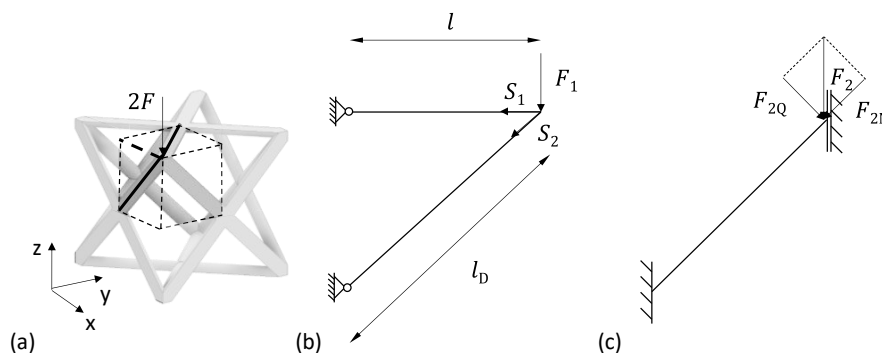


Figure 6. FCC strut lattice elementary cell (a) first force path calculated as a framework (b) second force path calculated as bending beam clamped on both sides (c)

- The diagonal strut of the FCC cell in the x-y-plane is projected to the x-z-plane with the respective fictive projected force
- Knots with several struts are assumed to behave similar to a soft clamping
- Knots are assumed to be significantly stiffer than free strut areas, and therefore reduce the effective length of the force paths
- Based on AlSi10Mg material properties are set to $E = 71\,000\text{ MPa}$ and $\nu = 0.3$

The given assumptions are described by the following equations for the calculation of the pressure stiffness. F_1 is the force acting on the framework and F_2 the force acting on the bending beam. K_{F1} and K_{F2} are the corresponding pressure stiffnesses of the two force paths and the overall pressure stiffness K_{pressure} is the sum of the partial stiffnesses. Table 1 shows the results of the analytical calculation.

$$F = F_1 + F_2 \tag{2}$$

$$w_{\text{framework}} = w_{T/P} \tag{3}$$

$$w_{B,\text{total}} = w_B + w_S + w_\varphi + w_N \tag{4}$$

w_N : lowering in consequence of normal force deformation

w_B : deflection in consequence of beam bending

w_S : shear deformation

w_φ : deflection in consequence of soft clamping at the knot

$$K_{F1} = \frac{F_1}{w_{T/P}} \quad (5)$$

$$K_{F2} = \frac{F_2}{w_{B,\text{total}}} \quad (6)$$

$$K_{\text{pressure}} = K_{F1} + K_{F2} \quad (7)$$

Table 1. Results of analytical and simulative pressure stiffness calculation and their relation

relative density	d/l FCC	$K_{\text{pressure,analy}}$ in MPa FCC	$K_{\text{pressure,sim}}$ in MPa FCC	$\frac{K_{\text{analy}}}{K_{\text{sim}}}$ FCC	d/l BCC	$K_{\text{pressure,analy}}$ in MPa BCC	$K_{\text{pressure,sim}}$ in MPa BCC	$\frac{K_{\text{analy}}}{K_{\text{sim}}}$ BCC
0.05	0.09	535.34	499	1.07	0.10	25.87	26	1.01
0.1	0.13	1199.50	1152	1.04	0.15	127.58	127	1.00
0.15	0.16	1993.97	1974	1.01	0.18	340.41	340	1.00
0.2	0.19	2939.84	2994	0.98	0.21	704.58	704	1.00
0.25	0.22	4057.81	4247	0.95	0.24	1264.19	1267	1.00
0.3	0.25	5384.32	5770	0.93	0.27	2077.62	2078	1.00
0.35	0.27	6962.82	7602	0.92	0.30	3205.22	3199	1.00
0.4	0.29	8853.59	9788	0.90	0.32	4721.55	4692	1.01
0.45	0.32	11134.91	12360	0.90	0.35	6623.97	6630	1.00
0.5	0.34	13903.33	15363	0.90	0.37	9307.09	9086	1.02

As visible in Table 1, the analytical calculations provide suitable results with a deviation of up to 10%. The calculation of the BCC cell proves the assumption of the bending beam clamped on both sides with the additional consideration of shear deformation and compression through a normal force to be an appropriate approximation for the analytical description of diagonal struts in meso cells. Furthermore, the influence of the soft clamping the knot represents compared to the fixed clamping within the bending curve has to be considered by impinging the knot area with a bending deformation, hence contortion. The results of the calculation of the FCC cell show that an analytical calculation by addition and superposition of the partial stiffnesses of single struts or substructures is possible and the approach to project struts within the x-y-plane as well as their displacements and forces to the x-z-plane or y-z-plane is valid. This means that dividing the flow of force into two independent paths to determine the partial forces and stiffnesses is applicable while the overall force is the superposition of the partial forces and the stiffness is the sum of the partial stiffnesses. To figure out the relation of the forces and consequently stiffnesses a matching condition is applicable, which, in this case, is the identical horizontal displacement for both paths.

5. Discussion

The results of the analytical calculation and the FE-simulation of the pressure stiffness of the strut lattice cells agree with less than or equal to 10% deviation. The close agreement of the analytical calculation and the simulation allows conclusions about underlying effects automatically represented in the FEM but overlaying in a way they cannot separately be examined. Based on the identified effects the mathematical description using power fits is adjusted.

5.1. Influences and effects of elementary cells on the pressure stiffness

Comparing the simulation results and the analytical calculation provides overlaying effects and influences within the strut lattice cells and allows a deeper understanding of influencing parameters and their effects on the elementary cell's properties. As deducible from the separation of force paths within the quaver FCC cell, tension and pressure as well as bending and shear act within the struts. Shear has to be taken into account because especially the thicker struts are stocky and therefore shear deformation has a significant impact on the overall deformation. In Figure 7 the simulated results, the overall analytical pressure stiffness

and the partial pressure stiffnesses of the framework K_{F1} and the bending beam K_{F2} are plotted. The comparison shows that the FE-simulation and the analytical calculation are in accordance. Furthermore, for small ratios d/l the framework stiffness K_{F1} , which is based on tensile and pressure stiffness, outweighs while the bending and shear stiffness of the bending beam are close to zero. The dominant tensile/pressure stiffness is effective till a d/l ratio of 0.16, which for FCC strut lattices corresponds to 15% relative density. For $0.16 \leq d/l \leq 0.26$, 15 – 35% relative density, respectively, the tensile/pressure stiffness and the bending/shear stiffness increase with similar slope and overlay. Above d/l of 0.26, hence 35% relative density, the bending stiffness overly increases and dominates the slope of the stiffness curve, though tensile/pressure stiffness still contributes significantly.

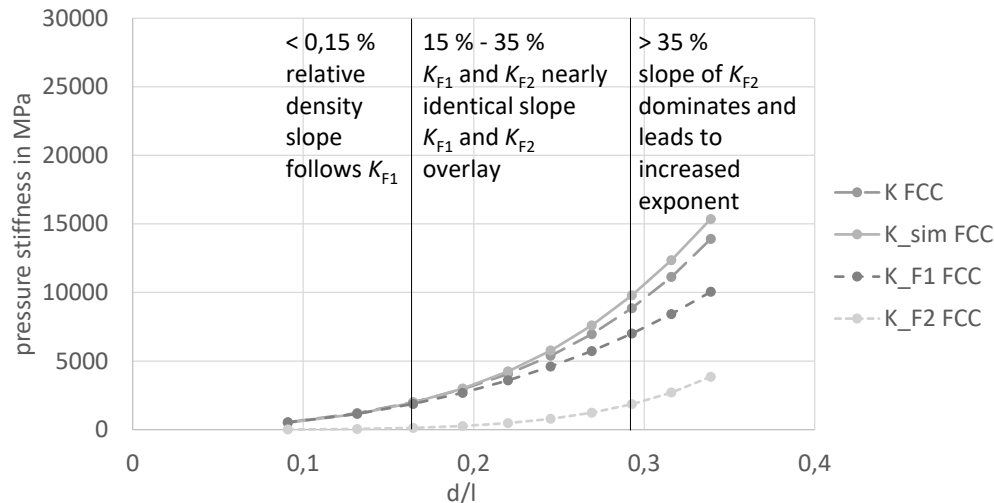


Figure 7. Comparison of partial compression stiffnesses, analytical and simulated stiffnesses and identification of areas of different dominating effects impacting the stiffness

Further effects become relevant in the strut compound in the FCC and the BCC cell. The *agglomerate effect* describes the mass accumulation in the areas of knots, which leads to a significantly higher local stiffness compared to the free strut length. The increased stiffness stems from the larger cross section and the isostatic pressure conditions that causes a restriction of deformation. Thus, the knot areas contribute to the overall stiffness on one hand by their significantly higher structural stiffness and on the other hand through the deformation hindrance of the attached struts. Examining the BCC cell reveals that the deformation hindrance does not correspond to a rigid structure like the bending curve of the double-sided clamped beam describes, but provides only part of the self-aligning torque, which would hold the clamped beam end in its exact starting angle. Therefore the knot area acts like a *soft clamping*. The area of the strut influenced by the knot is about 4% of the bending beam length, which is impinged with the shear contortion. The stiffer knot areas furthermore cause a *reduction of the effective length* for the tension and pressure as well as for the bending and shear deformation. The reduction amounts about the strut diameter per knot for tension and shear and 1.5 times the strut diameter for bending. Considering this amount of reduction, the presented calculation results are achieved. The *interaction of neighbouring elementary cells* that is represented by the PBC in the FEM partly manifests within the agglomerate effect because struts of neighbouring cells contribute to the local mass accumulation and the isostatic pressure condition in the knot areas. Furthermore, interaction effects go into the half thickness of edge and face struts. The knowledge of these effects allows a purposeful design or adaption of elementary cells according to requirements for stiffness by utilising the impact of the effects. E.g. increasing the amount of material in the knot area instead of the whole struts increases the stiffness of a cell with less material expense.

5.2. Choice of mathematical description for pressure stiffness scaling

Considering the physical background, the power fit has been chosen as the most promising mathematical description of the scaling relation between d/l ratio and the pressure stiffness. The power fit suits the BCC cell's stiffness with $R^2 = 0.99$. However, it does not match the simulation

results in the boundary areas of the d/l ratio for the FCC cell, which is traced back to the overlaying stress conditions within the cell. Based on the conclusions from the comparison of simulation and analytical calculation in Figure 7 that show the different dominating effects, the fit is separated into three areas with different power fits according to these effects as shown in Figure 8. For the applicability of the mathematical description for the design of meso structures, it is necessary to consider manufacturing influences like material and build direction. So far, the mathematical description provides the possibility to identify the required strut thickness for a certain stiffness coming from the simulation of the used cell with the used material inputs. To match the practical stiffness results at the best the material parameters have to be taken from printed parts with the applied build direction. Hence, for meso structures oriented transversely to the build direction the transverse material stiffness and Poisson's ratio should be used within the simulation.

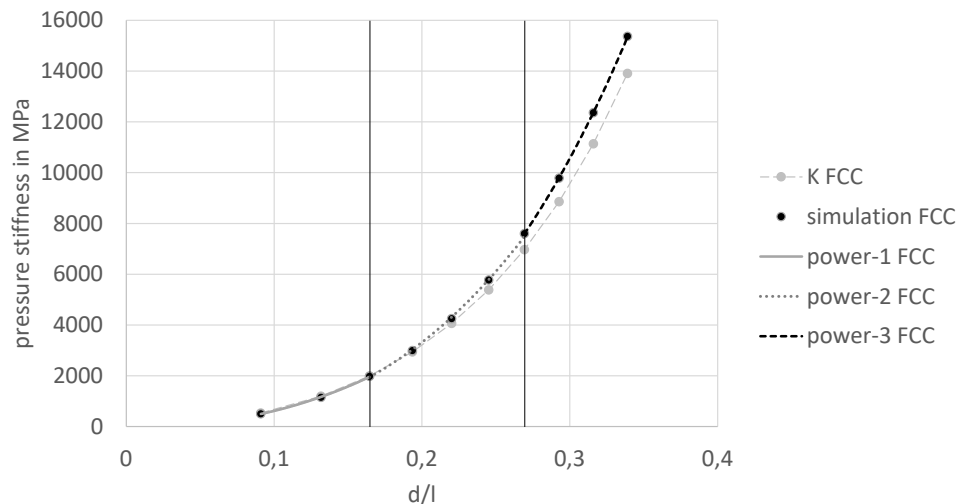


Figure 8. Partial fit of pressure stiffness simulation results

6. Conclusion and Outlook

Based on a FE-simulation of the pressure stiffness of strut-based meso structures a power fit has been identified as a mathematical description to scale the meso structures' stiffness depending on the influencing parameter of structural thickness and elementary cell size. This scaling model serves as an alternative to iteratively determining the influencing parameters for a required stiffness using FEM. Based on an analytical calculation of FCC and BCC lattice structures underlying effects to the pressure behaviour of strut lattices are identified. Considering these effects the mathematical description is revised accordingly by subdividing the fit into three fits that show improved agreement to the simulation.

For further research, this approach shall be transferred to other load cases like shear, bending or torsion and other meso structure types. Furthermore, the mathematical model shall be extended for asymmetric cells which requires the inclusion of further influencing parameters like the ratios of the cell edge lengths. Moreover, meso structures can be graded between neighbouring cells but also in its structural thickness which requires a description depending on a variable structural thickness. For dimensioning a meso structure, a calculation model for the strength and buckling resistance is required additionally.

References

- Becker, W. and Gross, D. (2002), *Mechanik elastischer Körper und Strukturen*, Berlin, Heidelberg, s.l., Springer Berlin Heidelberg. <https://dx.doi.org/10.1007/978-3-642-56124-5>
- Cheng, L., Liang, X., Belski, E., Wang, X., Sietins, et al. (2018), "Natural Frequency Optimization of Variable-Density Additive Manufactured Lattice Structure: Theory and Experimental Validation", *Journal of Manufacturing Science and Engineering*, Vol. 140, No. 10, p. 952. <https://dx.doi.org/10.1115/1.4040622>
- Cheng, L., Zhang, P., Biyikli, E., Bai, J., Robbins, J. and To, A. (2017), "Efficient design optimization of variable-density cellular structures for additive manufacturing: theory and experimental validation", *Rapid Prototyping Journal*, Vol. 23, No. 4, pp. 660–677. <https://dx.doi.org/10.1108/RPJ-04-2016-0069>

- Crupi, V., Kara, E., Epasto, G., Guglielmino, E. and Aykul, H. (2017), "Static behavior of lattice structures produced via direct metal laser sintering technology", *Materials & Design*, Vol. 135, No. 4, pp. 246–256. <https://dx.doi.org/10.1016/j.matdes.2017.09.003>
- Dassault Systèmes SE: Abaqus/CAE. 2020.
- Dong, G., Tang, Y. and Zhao, Y. F. (2017), "A Survey of Modeling of Lattice Structures Fabricated by Additive Manufacturing", *Journal of Mechanical Design*, Vol. 139, No. 10, p. 187. <https://dx.doi.org/10.1115/1.4037305>
- Ge, C., Priyadarshini, L., Cormier, D., Pan, L., Tuber, J. (2018), "A preliminary study of cushion properties of a 3D printed thermoplastic polyurethane Kelvin foam", *Packaging Technology and Science*, Vol. 31 No. 5, S. 361–368. <https://dx.doi.org/10.1002/pts.2330>.
- Gibson, L. J. and Ashby, M. F. (2014), *Cellular Solids - Structure and properties*, 2. ed., Cambridge solid state science series. Cambridge University Press, Cambridge. <https://doi.org/10.1017/CBO9781139878326>
- Hao, L., Raymont, D., Yan, C., Hussein, A. and Young, P. (2011) "Design and additive manufacturing of cellular lattice structures", *Innovative Developments in Virtual and Physical Prototyping*, CRC Press, pp. 249–254. <https://dx.doi.org/10.1201/b11341-40>
- Hradetzky, J. (1978), *Das Bestimmtheitsmaß*, Forstwissenschaftliches Centralblatt, Vol. 97, No. 1, pp. 168–181. <https://dx.doi.org/10.1007/BF02741104>
- Lachmayer, R. and Lippert, R. B. (2020), *Entwicklungsmethodik für die Additive Fertigung*, Berlin, Springer Berlin; Springer Vieweg. <https://dx.doi.org/10.1007/978-3-662-59789-7>
- Maconachie, T., Leary, M., Lozanovski, B., Zhang, X., Qian, M. et al. (2019), "SLM lattice structures: Properties, performance, applications and challenges", *Materials & Design*, Vol. 183, No. 3, p. 108137. <https://dx.doi.org/10.1016/j.matdes.2019.108137>
- Nguyen, C. H. P., Kim, Y. and Choi, Y. (2021) "Design for Additive Manufacturing of Functionally Graded Lattice Structures: A Design Method with Process Induced Anisotropy Consideration", *International Journal of Precision Engineering and Manufacturing-Green Technology*, Vol. 8, No. 1, pp. 29–45. <https://dx.doi.org/10.1007/s40684-019-00173-7>
- Nguyen, J., Park, S.-i. and Rosen, D. (2013) "Heuristic optimization method for cellular structure design of light weight components", *International Journal of Precision Engineering and Manufacturing*, Vol. 14, No. 6, pp. 1071–1078. <https://dx.doi.org/10.1007/s12541-013-0144-5>
- Ruiz de Galarreta, S., Jeffers, J. R.T. and Ghouse, S. (2020) "A validated finite element analysis procedure for porous structures", *Materials & Design*, Vol. 189, p. 108546. <https://dx.doi.org/10.1016/j.matdes.2020.108546>
- Schulte, F. and Kirchner, E. (2021) "Ansatz zur belastungsgerechten Auslegung additiv gefertigter Meso-Strukturen in Bauteilen", *Proceedings of the 32nd Symposium Design for X, 27 and 28 September 2021*, The Design Society. <https://dx.doi.org/10.35199/dfx2021.16>
- Shi, X., Liao, W., Liu, T., Zhang, C., Li, D., Jiang, W. et al. (2021) "Design optimization of multimorphology surface-based lattice structures with density gradients", *The International Journal of Advanced Manufacturing Technology*, Vol. 117, No. 7-8, pp. 2013–2028. <https://dx.doi.org/10.1007/s00170-021-07175-3>
- Smith, M., Guan, Z. and Cantwell, W. J. (2013) "Finite element modelling of the compressive response of lattice structures manufactured using the selective laser melting technique", *International Journal of Mechanical Sciences*, Vol. 67, No. 36–37, pp. 28–41. <https://dx.doi.org/10.1016/j.ijmecsci.2012.12.004>
- Steffan, K.-E. W. H., Fett, M. and Kirchner, E. (2020) "Extended approach to optimize modular product through the potentials of additive manufacturing", *Proceedings of the Design Society: DESIGN Conference*, Vol. 1, pp. 1115–1124. <https://dx.doi.org/10.1017/dsd.2020.172>
- Steffan, K.-E., Fett, M., Kurth, D. and Kirchner, E. (2021) "Identification of optimization areas of a transtibial prosthesis through the potentials of additive manufacturing processes" *Proceedings of the Design Society*, Vol. 1, pp. 1807–1816. <https://dx.doi.org/10.1017/pds.2021.442>
- Vega-Moreno, A., Tenegi Sanginés, F., Márquez-Rodríguez, J. F., Calvo-Tovar, J., Schnetler, H., et al. (2020) "Design for additive manufacture (DfAM): the “equivalent continuum material” for cellular structures analysis", *Modeling, Systems Engineering, and Project Management for Astronomy IX*. Online Only, United States, 14.12.2020 - 18.12.2020, SPIE, p. 84. <https://dx.doi.org/10.1117/12.2560999>
- Wang, X., Zhu, L., Sun, L. and Li, N. (2020) "A study of functionally graded lattice structural design and optimisation", *6th International Conference on Mechanical Engineering and Automation Science (ICMEAS)*. Moscow, Russia, 29.10.2020 - 31.10.2020, IEEE, pp. 50–55. <https://dx.doi.org/10.1109/icmeas51739.2020.00017>
- Xu, S., Shen, J., Zhou, S., Huang, X. and Xie, Y. M. (2016) "Design of lattice structures with controlled anisotropy", *Materials & Design*, Vol. 93, pp. 443–447. <https://dx.doi.org/10.1016/j.matdes.2016.01.007>